

## Measurement of the $\beta$ -energy spectrum of $^3\text{H}$ to determine the antineutrino mass

J. J. Simpson

*Department of Physics, University of Guelph, Guelph, Ontario N1G 2W1, Canada*

(Received 18 August 1980)

An experiment to measure the  $\beta$ -energy spectrum of tritium implanted at high energy into a Si(Li) x-ray detector has been carried out primarily with the aim of determining the mass of the electron antineutrino, but also the extrapolated end-point energy of the  $\beta$  spectrum. The measurement implies a mass  $< 65$  eV with 95% confidence and a best value of 20 eV which is however only 0.2 standard deviations from zero mass. The end-point energy is  $18\,567 \pm 5$  eV. A discussion of atomic effects which are important for calculating the  $^3\text{H}$ - $^3\text{He}$  atomic-mass difference from the end-point energy is presented, as well as a discussion on the possibility of improving the limit on the antineutrino mass in the present type of experiment.

### I. INTRODUCTION

The precision measurement of the  $\beta$  spectrum of tritium near its end point seems to offer the best chance of determining, or putting a useful limit on, the mass  $m_{\bar{\nu}}$  of the electron antineutrino. Over the years, a fair number of measurements of this spectrum, tabulated in papers by Bergkvist<sup>1</sup> and Piel,<sup>2</sup> have been carried out and recently a new experiment<sup>3</sup> has been reported claiming an improved result. Without exception, the experiments which achieve the lowest limit for  $m_{\bar{\nu}}$  use some type of magnetic  $\beta$  spectrometer to measure the electron's momentum distribution over a limited region near the end point. Although these instruments achieve good resolution ( $\sim 50$  eV) which is desirable for determining  $m_{\bar{\nu}}$ , they have other experimental problems connected with the geometry and thickness of the high-activity source required, background problems from multiple scattering and, as Bergkvist points out in his classic papers,<sup>1</sup> uncertainties associated with effects of final-state interactions. However, even after all known experimental corrections have been made, there still remains in the best of these measurements<sup>1,3</sup> a residuum of uncertainty. In the measurements of Bergkvist<sup>1</sup> the Kurie plots of his data showed an unexpected curvature which had to be taken into account in a phenomenological way, and in those of Tret'yakov *et al.*<sup>3</sup> the fit of their data was bad, having a  $\chi^2$  of 284 with 191 degrees of freedom. This was accounted for by assuming that nonstatistical variations make the actual errors larger than the statistical errors by 20%. There is also in both experiments the problem of the final atomic/molecular states which are available to the decay. These states may have energy differences appropriate to the helium ion, i.e., in the region of 25–50 eV or so, and consequently limits on  $m_{\bar{\nu}}$  less than about 50 eV might not be very meaningful without assessing carefully

the probabilities of various final states. Clearly, it would be nice to have an experiment different from the above, yet accurate enough to check the present limit on  $m_{\bar{\nu}}$ .

The availability of a high-energy tritium beam from a tandem Van de Graaff accelerator and improved detector technology suggested a different type of experiment. The basic idea is the measurement of the  $\beta$ -particle energy spectrum of tritium implanted in a Si(Li) x-ray detector. Source effects and final-state interactions are now quite different from those in the magnetic-spectrometer experiments. The major disadvantage of this method is the considerably worse resolution of the Si(Li) detector ( $\sim 300$  eV) but, as we shall see, this disadvantage can be circumvented to a large extent. A preliminary report of this work has been presented to the conference Neutrino '79 in Bergen.<sup>4</sup>

It appears that only one previous attempt to use a Si(Li) detector to measure the  $\beta$  spectrum of implanted tritium has been carried out.<sup>5</sup> However, it was not possible in that experiment to infer a useful limit on the antineutrino mass because of a very high x-ray background and rather poor resolution of detector.

As well as putting a limit on the antineutrino mass, the study of the  $\beta$ -ray end point can be used to look for a possible universal neutrino or antineutrino degeneracy.<sup>6</sup> Also, the absolute value of the atomic-mass difference between  $^3\text{H}$  and  $^3\text{He}$  can be inferred in principle from the end-point energy, and there will be some discussion of this.

In the following, the word neutrino may sometimes be used when antineutrino is meant and when no ambiguity arises.

### II. GENERAL CONSIDERATIONS

There are some general considerations which dictate many features of the design of the experi-

ment.

In order to achieve the best result, one would like the best resolution obtainable at 18.6 keV energy. At the present time this is obtained with cooled Si(Li) detectors of small cross-sectional area ( $\sim 30 \text{ mm}^2$ ). In principle, high-purity germanium crystals should be capable of achieving better resolution because of a small Fano factor and lower electron-hole pair-creation energy,<sup>7</sup> but this has not yet been realized.

Other requirements, however, conflict with the aim of best resolution. Because the neutrino mass manifests itself in a distortion of the  $\beta$  spectrum at and near the end point, high source activity is required, corresponding to large implantation doses. In order to achieve the latter and avoid unacceptable radiation damage, a larger area detector than that giving the best resolution is appropriate. The reason is that, while the count rate achievable is proportional to the area of the detector, the resolution in the energy region of importance does not change much with the area because it is primarily determined by statistical factors and not by electronic noise<sup>7</sup> (see also Appendix A).

Another feature which makes the use of a Si(Li) detector desirable, in spite of a possible resolution improvement with intrinsic germanium, is the low energy of the silicon  $K$  x-ray (1.7 keV) compared to that of germanium (9.9 keV). An x-ray spectrum in the germanium detector, for energies above the  $K$ -absorption edge, features a  $K$ -escape peak whose magnitude will be energy dependent and which may, therefore, seriously complicate the detector's resolution function which is needed to extract the neutrino mass (see below). This problem is much less serious in a Si(Li) detector because of the much lower energy of the  $K$ -absorption edge and can be avoided completely in the  $\beta$  spectrum by implanting much deeper than the absorption length of Si  $K$  x rays ( $\sim 14 \mu\text{m}$ ).

The calibration of the detector and the resolution function can be measured with x rays at the relevant energies, 10 to 20 keV, because they interact via the photoelectric effect, ejecting a high-energy photoelectron which, to the detector, is indistinguishable from a  $\beta$  particle. There is the difference, however, that x rays generally enter the crystal from one direction, usually parallel to the electric field, whereas the internal source emits its  $\beta$  particles isotropically. Since, in the former case, the photoelectrons will be preferentially ejected in the direction of the incident x-ray photon they would thus gain or lose a small amount of energy depending on the direction of the electric field. This effect has apparently been observed for  $\gamma$  rays in planar Ge(Li) detectors.<sup>8</sup> In the pres-

ent case, however, the range of the ejected photoelectrons is so short ( $< 2.5 \mu\text{m}$ ) that the energy gained or lost in falling or rising in the electric field will be less than about 0.5 eV.

Another phenomenon which must be considered in the resolution function is bremsstrahlung, both internal<sup>9</sup> and external,<sup>10</sup> which may be emitted as the  $\beta$  particle leaves the field of the decaying nucleus or slows down in the detector material. Because of the low energy of the  $\beta$  particles, and because of the low  $Z$  in the case of external bremsstrahlung, the energy lost to bremsstrahlung is very small. More important, however, is the fact that the tritium can be implanted at sufficient depth to reabsorb the bulk of the bremsstrahlung photons which are very low energy.

As suggested above, it is desirable to implant the tritium atoms deeply compared to the absorption length of the Si  $K$  x rays (and hence deeply compared to the  $\beta$  range also). Furthermore, to simplify experimental problems and to avoid surface contamination of the Si(Li) crystal it also seems desirable to make the implantation through the thin beryllium window which usually covers the crystal. For a typical window thickness of about 0.025 mm a minimum energy of tritium beam of about 6 MeV is required for sufficient depth of implantation. Such beams are available from tandem Van de Graaff accelerators.

Nuclear scattering can, in principle, lead to tritium atoms stopping near ( $\sim 10 \mu\text{m}$ ) the surface provided the scattering occurs in the first 70  $\mu\text{m}$  of the tritium path. A rough estimate is that less than  $\sim 10^{-7}$  of the tritium atoms by fraction would be near the surface.

One wants to avoid or circumvent radiation damage and still have a high count rate. There has been work on radiation damage caused by proton bombardment in silicon in connection with work on solar cells<sup>11</sup> but the amount of radiation damage a solar cell can withstand and still function is probably somewhat in excess of that which a detector can tolerate and still operate with reasonable resolution. The present experiment therefore provides some information about the latter.

### III. EXPERIMENTAL DETAILS

#### A. Tritium implantation

The detector in which the tritium was implanted is an 80 mm<sup>2</sup>, 5-mm-thick Si(Li) detector with a pulsed optical-feedback preamplifier.<sup>12</sup> By modern standards the resolution is modest, about 215 eV at 5.9 keV. It is mounted in a horizontal cryostat, and has on the front a 0.025-mm-thick beryllium window, 11 mm in diameter, to minimize absorption of x rays.

An x-ray scan across the detector showed that the sensitive area was centrally located in its cryostat to an accuracy of about 1 mm. An 8-mm-diameter collimator of 0.25-mm-thick tantalum was placed on the end of the cryostat to make sure that the tritium was implanted away from the edges of the sensitive volume.

The tritium beam used for the implantation was obtained from the FN tandem Van de Graaff accelerator at McMaster University. A diffuse beam, about 6 mm in diameter, passed through a 0.013-mm-thick tantalum window at the end of a beam pipe and, after a short distance in air, into the detector through its beryllium window (Fig. 1). Beam current was kept to about 0.25 nA, and the beam energy was varied from 8.0 to 9.1 MeV in steps of 100 keV. These energies give an implantation depth of about 0.2 mm which is large compared to the range of the 18.6 keV  $\beta$  particles ( $\sim 2.5 \mu\text{m}$ ) and to the absorption length of Si x rays ( $\sim 14 \mu\text{m}$ ). During implantation the detector was kept at liquid-nitrogen temperature. After a number of short beam bursts, each one at a different energy, the detector was reconnected to its bias and preamplifier supplies and the resolution of the 14.4-keV  $\gamma$  ray of  $^{57}\text{Fe}$  was examined. It was observed that at some point during implantation the  $\gamma$  ray began to develop a tail on its low-energy side and implantation was stopped. The  $\beta$ -ray count rate was about 70 counts per second at the end. The tritium atomic density at implantation is estimated to be  $\sim 1.5 \times 10^{13} \text{ cm}^{-3}$ .

### B. Spectrum recording

For calibration and stabilization the  $\beta$  spectrum is recorded with x rays in the following way. A strong  $^{109}\text{Cd}$  source, which emits an 87.7-keV  $\gamma$  ray and the x rays of Ag, is used to fluoresce foils of Cu and Mo. This source is in the shape of an annulus so that fluorescence can be observed at  $180^\circ$ , considerably reducing the unwanted background from both the  $\gamma$  ray and Ag x rays. Between the source and Si(Li) detector (see Fig. 2) there is a slotted wheel, made of layers of lead, cadmium, copper and aluminum, which serves as an x-ray chopper. The wheel rotates with a period of a few seconds, and a signal, which routes the pulses from the detector into either one half of a 4096-channel memory of a multichannel analyzer or the other, is generated from the position of the chopper. Thus one spectrum in the analyzer contains a spectrum of  $\beta$  rays plus x rays transmitted through the slots, and the other  $\beta$  rays only. Both spectra, however, are recorded through the same analog-to-digital converter and the routing is done purely digitally. The end of the cryostat, with the

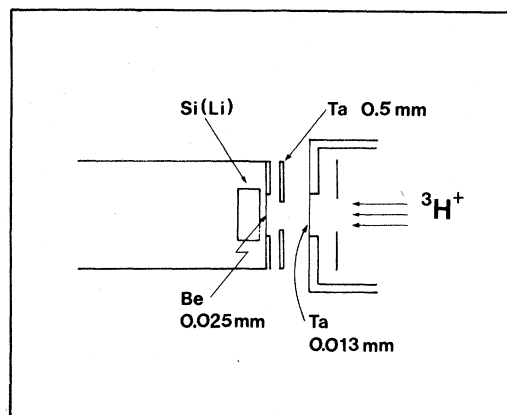


FIG. 1. Procedure used for implanting tritium into a commercially obtained Si(Li) x-ray detector.

exception of the entry window, was also shielded with lead and cadmium foil. An example of the spectra is shown in Fig. 3.

During recording of the  $\beta$  spectrum and  $\beta$  plus x-ray spectrum, a digital gain stabilizer is used on the Mo  $K_\alpha$  x ray. Over periods of weeks, the position of the stabilizing line, as measured by its centroid, never moved by more than about 2 eV. There were small drifts in the position of the  $K_\alpha$

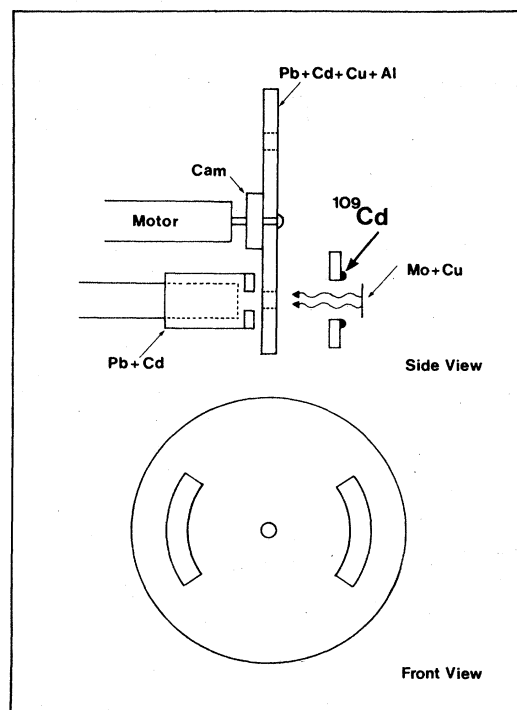


FIG. 2. X-ray chopper and shielding arrangement for providing intermittent x rays for calibration and stabilization and for resolution-function measurements.

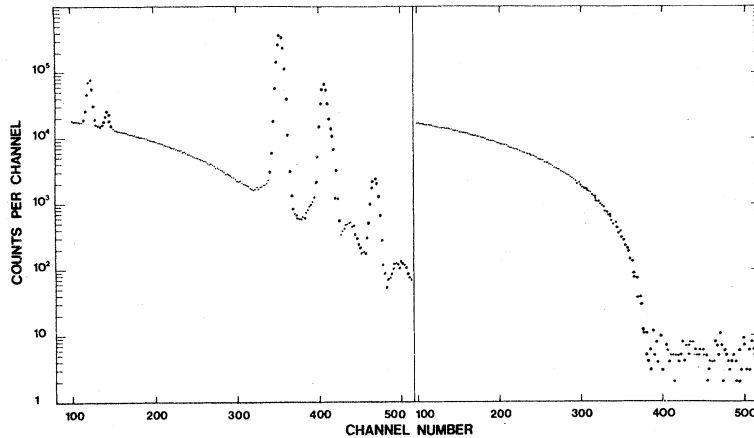


FIG. 3. Logarithmic display of a typical spectrum in the multichannel analyzer. Approximately 40 eV/channel. The x rays shown are those of Cu, Mo, and Ag. The ability of the chopper system to cut off the x rays is immediately apparent.

x ray of Cu, amounting sometimes to about 20 eV in the same period.

A pulse-pileup inspector looks at fast pulses derived from the preamplifier signals. When two or more pulses occur within the inspection time of 16  $\mu$ s, the multichannel analyzer is gated off for 32  $\mu$ s. A time constant of 6  $\mu$ s is used in the linear amplifier. Missed pileup pulses are estimated to be less than the statistical error on the background. The multichannel analyzer was also gated off during the reset pulse of the preamplifier.

After the tritium implantation, spectra were taken for some weeks with a bias voltage of 1000 V on the detector, as recommended by the manufacturer. The spectra were recorded at intervals of a few days on magnetic tape. Because Lewis<sup>5</sup> had observed a change in end-point energy with bias voltage, the bias on the detector was increased to 1500 V and another run of about one week was carried out. There was no apparent difference in end-point energy (see below). It was not possible to go to bias voltages lower than 800 V because of a very rapid worsening resolution, presumably due to bad charge collection.

As mentioned above, the resolution had deteriorated at the end of the implantation. An example, for the  $K_{\alpha}$  x-ray doublet of Mo, is shown in Fig. 4(a). It was then decided to attempt a short, gentle annealing of the detector with the gratifying results shown in Fig. 4(b); the resolution and line shape have returned to their preimplantation values. In a spectrum taken before implantation, the resolution [full width at half maximum (FWHM)] of the 5.9-keV x ray from <sup>55</sup>Fe was  $216.4 \pm 0.4$  eV, after implantation but before annealing it was about 240

eV, and after annealing it returned to  $217.1 \pm 1.1$  eV. Furthermore, the count rate in the  $\beta$  spectrum between the Cu and the Mo  $K_{\alpha}$  x-ray peaks was the same, to within 1%, as prior to annealing. A subsequent set of runs, at 1000 V bias, has been carried out in this postannealing stage. There is a significant change in the end-point energy, however, as a result of annealing (see below).

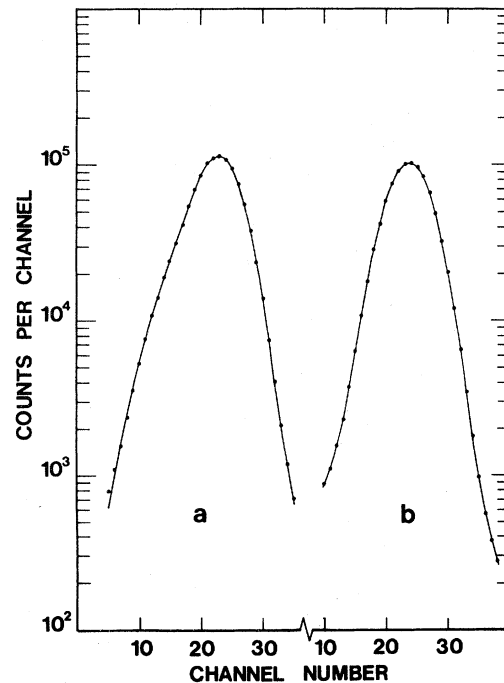


FIG. 4. Shape of the Mo  $K_{\alpha}$  doublet obtained during preannealing (a) and a postannealing run (b).

## IV. EXPERIMENTAL RESULTS

## A. Energy calibration

The x rays used for energy calibration are listed in Table I. The x-ray energies have been calculated from the compilations of x-ray energies of Bearden<sup>13</sup> and relative intensities of Scofield.<sup>14</sup>

Although the spectra were recorded with a dispersion of about 10 eV, it was felt that the resolution did not warrant such a dispersion, and the spectra have been compressed by adding together four adjacent channels.

The peak centroids are used as a measure of the energy. The centroids are determined after the shape of the  $\beta$  spectrum has been subtracted from the x-ray plus  $\beta$  spectrum. The rms deviation for a linear fit to the calibration points was always less than 2 eV.

## B. Resolution function

The resolution function for each run has been determined from the Cu  $K_\alpha$  and Mo  $K_\alpha$  x-ray lines collected at the same time, while the energy variation of the resolution has been checked in separate experiments with the addition of  ${}^{55}\text{Fe}$  x rays, the 14.4-keV  $\gamma$  ray of  ${}^{57}\text{Fe}$  and the  $K_\alpha$  x ray of Ag. The bremsstrahlung contribution to the resolution function in the present case is insignificant because at the depth of implantation there is essentially complete absorption for photons of less than 5 keV. It is estimated that bremsstrahlung gives rise to a degraded  $\beta$  pulse in less than one event in  $10^5$ . Experimentally, the resolution varied approximately linearly with energy, and this energy variation of the resolution is used in the analysis. The exact energy variation of the resolution is unimportant, however, since using a resolution function appropriate for 18.6 keV, as determined from the Mo  $K_\alpha$  line with allowance for the energy variation, over the whole of the fitting region changes the results by much less than statistical errors (see below).

Most important in determining the shape of the spectrum near the end point is the resolution there. This is primarily determined by the Mo  $K_\alpha$  x-ray doublet. The separation and relative intensity of the two components are constrained to agree with their known values<sup>13,14</sup> and the resolution function for each component is taken to be the sum of two Gaussian functions with independently varying height, width, and position. Examples of the four-Gaussian fit are given in Fig. 4 and the parameters of typical resolution functions of one component for both the preannealing and postannealing stages are given in Table II.

TABLE I. X-ray energies used for calibration.

Element	x-ray line	x-ray energy (keV)
Cu	$K_\alpha$	8.0410
Cu	$K_\beta$	8.905
Mo	$K_\alpha$	17.4432
Mo	$K'_{\beta_1} + K'_{\beta_2}$	19.650
Ag	$K_\alpha$	22.1031

The  $\beta$ -ray resolution function at 18.6 keV is obtained by increasing the values of both widths ( $\sigma$ ) by the observed energy variation between 17.44 and 18.6 keV, a 2% change, and by decreasing the widths by 1.1% to correct for the 6.8-eV Lorentzian linewidth of the Mo  $K_\alpha$  x rays.

## C. Analysis procedure

The experimental  $\beta$  spectra and Kurie plots were obtained after subtraction of a linear background determined from the region between the end point and about 23.5 keV. The background count rate at the end point is about  $9 \times 10^{-7} \text{ s}^{-1} \text{ eV}^{-1}$  with a slope of  $1.5 \times 10^{-11} \text{ s}^{-1} \text{ eV}^{-2}$ .

The theoretical  $\beta$  spectrum and Kurie plot were calculated at the experimental energy points by convoluting the resolution function with the theoretical  $\beta$  spectrum<sup>9</sup>

$$N_\beta(E, Z) = C p E [(Q - E)^2 - m_\nu^2]^{1/2} (Q - E) F(E, Z). \quad (1)$$

$E$  and  $p$  are the total energy and momentum of the  $\beta$  particle,  $m_\nu$  is the antineutrino mass in energy units,  $Q$  is the total energy available for the transition, and  $C$  is a constant. This expression assumes that the interaction is  $V - A$  and parity is maximally violated.

A modified nonrelativistic Fermi function of the

TABLE II. Typical parameters for the resolution function of one component of the Mo  $K_\alpha$  x-ray corresponding to the data of Fig. 4. The resolution function is  $y = h_1 \exp[-(x - s_1)^2/2\sigma_1^2] + h_2 \exp[-(x - s_2)^2/2\sigma_2^2]$ .

	$\sigma_1$ (eV)	$h_2/h_1$	$\sigma_2$ (eV)	$(s_1 - s_2)$ (eV)
Preanneal	123	0.348	215	129
Postanneal	134	0.013	405	149

form

$$F(E, Z) = x(1 - e^{-x})^{-1} [1.002\,037 - 0.001\,427(v/c)],$$

where

$$x = \frac{2\pi Z\alpha}{v/c}$$

has been used. Here  $Z$  is the charge of the daughter nucleus,  $v/c$  is the  $\beta$ -particle speed relative to that of light, and  $\alpha$  is the fine-structure constant. The second term in brackets is a phenomenological modification which makes the nonrelativistic expression<sup>15</sup> yield the same values as the relativistic calculation of Behrens and Janecke<sup>16</sup> over the energy range of interest.

The constant  $C$  is determined for particular values of  $Q$  and  $m_{\bar{\nu}}$  by a least-squares fit of the data over the  $\beta$  kinetic-energy range from 9.5 to 17 keV. (The regions where background x rays might be present have thus been avoided in the fitting.) The end-point region, without further fitting or renormalization, is then used to test for an anti-neutrino mass.

The pulsed optical feedback preamplifier causes an energy-dependent dead time proportional to the kinetic energy of the  $\beta$  particles. The number of counts at each kinetic energy  $T_{\beta}$  has been corrected by a factor  $(1 - \tau T_{\beta})^{-1}$  and the value of  $\tau$  has been determined by least-squares fitting. In the preannealing runs  $\tau$  is  $(0.10 \pm 0.15) \text{ MeV}^{-1}$  and in the postannealing runs it is  $(0.45 \pm 0.20) \text{ MeV}^{-1}$ . This latter value is approximately in agreement with the value of  $0.6 \text{ MeV}^{-1}$  obtained by a Monte Carlo simulation of the dead-time effect.<sup>12</sup> The smaller value for the preannealing stage is perhaps associated with a higher detector leakage current resulting in less energy-dependent dead time. The error in  $\tau$  is included in the final results.

## V. RESULTS

The shape spectrum in Fig. 5, defined as the ratio of the observed to the theoretically expected number of counts, shows no anomalies over a

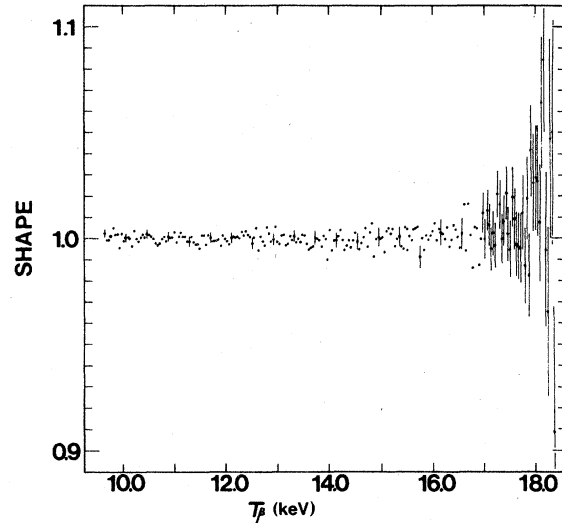


FIG. 5. A typical  $\beta$ -shape spectrum of tritium. The ordinate is the experimental number of counts divided by the theoretical number of counts after least-squares fitting. The abscissa is the kinetic energy of the  $\beta$  particles.

large section of the  $\beta$  spectrum. All the runs were comparably good as can be judged by the  $\chi^2$  values of the fits given in Tables III and IV.

The extrapolated end-point energy  $Q$  is also presented in Tables III and IV. There is included in the values of  $Q$  quoted a correction for a count-rate-dependent shift amounting to 17 eV. This correction was determined by using an x-ray chopper which attenuated the Mo  $K$  x rays by a factor of 5 rather than cutting them out completely. Note that there is no significant difference between values of the end-point energy obtained at 1000 and 1500 V bias. The end-point energy changes only by 1 eV in using the resolution function at 18.6 eV over the whole fitting region.

A comparison of Tables III and IV shows that there has been an increase in the extrapolated end-point energy of about 65 eV after annealing. This might be explained by attributing to the annealing procedure the disappearance of charge trapping

TABLE III. End-point energies and ratios  $R(m_{\bar{\nu}})$  of the tritium spectrum from the "preannealing" runs. The convoluted theoretical spectrum is fitted to the experimental over the energy range from 9.5 to 17 keV. Also given is  $\chi^2$  per degree of freedom.

Run	Bias voltage (V)	End-point energy (eV)	$\chi^2$	Confidence level	$R(m_{\bar{\nu}})$
1	1000	18 490 $\pm$ 5	1.017	43%	0.986 $\pm$ 0.024
2	1000	18 514 $\pm$ 7	0.854	92%	0.952 $\pm$ 0.044
3	1500	18 491 $\pm$ 6	0.961	64%	1.074 $\pm$ 0.038
4	1000	18 499 $\pm$ 6	1.026	37%	1.004 $\pm$ 0.040

TABLE IV. End-point energies and ratios  $R(m_{\bar{\nu}})$  of the tritium spectrum from the "postannealing" runs. The convoluted theoretical spectrum is fitted to the experimental over the energy range from 9.5 to 17 keV. Also given is  $\chi^2$  per degree of freedom.

Run	Bias voltage (V)	End-point energy (eV)	$\chi^2$	Confidence level	$R(m_{\bar{\nu}})$
1	1000	$18\,565 \pm 4$	0.921	77%	$1.008 \pm 0.025$
2	1000	$18\,565 \pm 5$	0.899	83%	$0.963 \pm 0.034$
3	1000	$18\,568 \pm 3$	0.938	72%	$0.999 \pm 0.016$

centers which were frozen in during implantation. However, the annealing does not, apparently, cause any loss of tritium from the sample, which is consistent with studies showing that, even at room temperature, implanted hydrogen remains immobile for long periods in both crystalline and amorphous silicon.<sup>17</sup>

The region near the end of the Kurie spectrum for both a preannealing and postannealing run is shown in Fig. 6 with the corresponding theoretical curves. It must be emphasized that the theory has *not* been renormalized to fit the end region, once again demonstrating that there are no unexplained systematic features at the present level of accuracy. There is no evidence of anomalous shape in the end-point region, and for  $m_{\bar{\nu}} = 0$  a reasonable value of  $\chi^2$  is obtained in the end-point region of all spectra. (All fits and  $\chi^2$  tests have been performed on the  $\beta$  spectra, not on the Kurie plots.) Furthermore, there appears to be no serious differential nonlinearity over the important

end region since, using the Cu and Mo  $K_{\alpha}$  x rays to determine a calibration line, the energies of the Mo  $K'_{\beta_1} + K'_{\beta_2}$  and Ag  $K_{\alpha}$  x rays are predicted correctly to an accuracy of better than 1 eV.

Taking the view that there is no uncertainty in  $\beta$ -decay theory, a powerful way to test for the antineutrino mass is to determine the number of counts in the  $\beta$  spectrum in a sensitive region near the end point where the only free parameter is  $m_{\bar{\nu}}$  (disregarding a universal neutrino degeneracy for the moment). The region selected which demonstrates the most sensitivity corresponds to about two resolution widths (FWHM) centered near the end-point energy. The results analyzed this way are presented in Fig. 7 and Tables III and IV. Here the number of counts in the experimental region and the number expected from the fit as a function of  $m_{\bar{\nu}}$  (corrected for binning) have been normalized to the expected number with  $m_{\bar{\nu}} = 0$  yielding the ratios  $R(m_{\bar{\nu}})$ . The errors are statistical. The number of counts in the background was

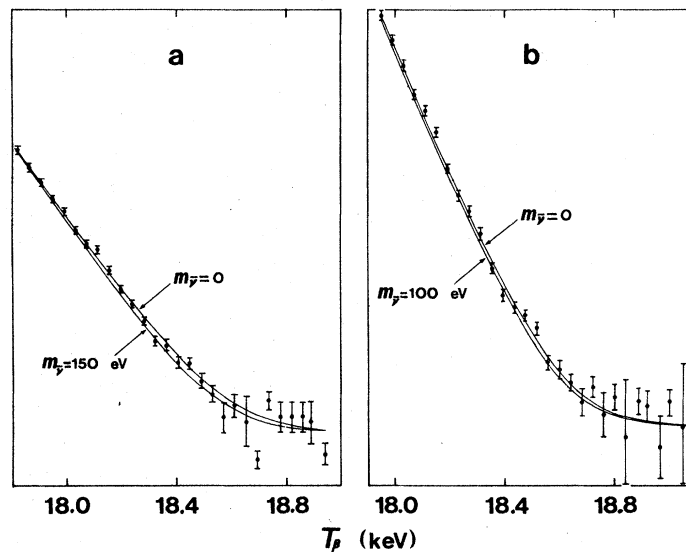


FIG. 6. Representative Kurie plots for a preannealing (a) and postannealing (b) run. The theoretical curves have not been fitted in the regions shown but are extrapolated from the  $\beta$  spectrum between 9.5 and 17 keV, as described in the text.

about 22% of the total. The use of an energy-independent resolution function, that corresponding to 18.6 keV, changes this ratio by only 0.1%. (See Appendix A for a simplified discussion of the sensitivity of this analysis method.)

This method of analysis is different from that employed in magnetic-spectrometer work.<sup>1,3</sup> There, because a very limited region near the end is measured, the shape of the spectrum is tested and resolution is at a premium. Here, a long portion of the  $\beta$  spectrum is relied upon to determine the expected  $\beta$  spectrum near the end, and hence somewhat worse resolution can be tolerated. Of course, better resolution would be advantageous here too.

## VI. DISCUSSION OF RESULTS

### A. Antineutrino mass

The experimental average value of  $R(m_{\bar{\nu}})$  for the preannealing runs is  $1.002 \pm 0.017$  and for the postannealing runs is  $0.996 \pm 0.013$ , the errors including the uncertainty in the nonlinearity correction  $r$ . Averaging these two together gives a ratio  $R(m_{\bar{\nu}})$  of  $0.998 \pm 0.011$  giving an antineutrino mass (Fig. 7) of 20 eV, 0.2 standard deviations from zero mass, with a 95% confidence interval implying  $m_{\bar{\nu}} < 65$  eV.

As seen in Table V, the present limit is comparable to the previous value of Bergkvist.<sup>1</sup> It is nominally worse than the value of Tretyakov *et al.*,<sup>3</sup> but it is not certain that, in considering only bound states of the  $^3\text{He}$  ion, all important final-state effects have been included by these authors. In his papers Bergkvist<sup>1</sup> shows how a magnetic-spectrometer system's effective resolution function is importantly and unmeasurably changed by final-state effects, and how important therefore

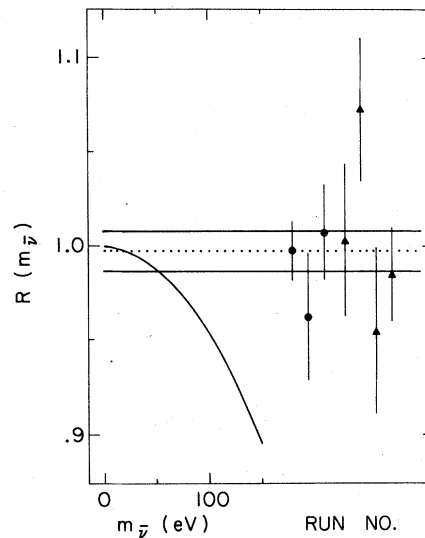


FIG. 7. The final results on  $m_{\bar{\nu}}$ . The ordinate is the number of counts in the sensitive region (see text) normalized to the theoretical number for  $m_{\bar{\nu}}=0$ . On the right are shown the results of the various runs (preannealing  $\blacktriangle$ , postannealing  $\bullet$ ). The horizontal dotted line is the weighted average of all runs, with a standard deviation shown by the horizontal continuous lines. On the left the smooth curve gives the calculated ratio  $R(m_{\bar{\nu}})$  as a function of  $m_{\bar{\nu}}$ .

it is to know the final state if one hopes to achieve mass limits comparable to energies associated with  $^3\text{He}$ , i.e.,  $\sim 25$ – $50$  eV. Arguments that final-state effects do not cause uncertainty in the present determination of  $m_{\bar{\nu}}$  are given in the next section.

### B. $^3\text{H}$ - $^3\text{He}$ mass difference

Table V lists the end-point energy obtained in the present experiment and in previous experi-

TABLE V. Comparison of experimental tritium end-point energies and antineutrino-mass limits.

Source	Reference	End-point energy (eV)	$^3\text{H}$ - $^3\text{He}$ atomic-mass difference (eV)	$m_{\bar{\nu}}$ (eV)
T implanted in Al	1	$18\,610 \pm 16$	$18\,651 \pm 16$	$<55$ (90% confidence)
Dextro-Levo-Leucine-4,5-T on Zapon	2	$18\,578 \pm 40$		$<100$ (no confidence limit)
Valine-T on Al	3	$18\,575 \pm 13$		$<35$ (90% confidence)
T implanted in Si(Li)	5	$18\,540 \pm 48$		
T implanted in Si(Li)	present	$18\,567 \pm 5$	$18\,567 \pm 5$	$<60$ (90% confidence)
Mass doublet	25		$18\,600 \pm 7$	

ments of comparable accuracy. The value obtained after annealing is used. It is certainly conceivable that this value might be systematically low, but probably only by an amount small compared to the change that occurred as a result of annealing. This is suggested by the fact that the resolution function returned to its preimplantation quality.

Because the previous experiments have been carried out with different types of tritium source, and the present experiment combines source and detector, it is necessary to compare a well-defined quantity such as the  $^3\text{H}$ - $^3\text{He}$  atomic-mass difference. In order to arrive at this, one must examine both the initial and final state of the decaying system.

### 1. Initial state

Deuterium implanted in a silicon crystal is found by channeling studies to occupy generally a well-defined and localized site in the tetragonal antibonding direction of the lattice about 1.6 Å from the nearest silicon atom.<sup>17,18</sup> Other evidence, such as infrared absorption measurements and the temperature dependence of hydrogen release, suggests that hydrogen is strongly chemically bonded to the silicon, perhaps in association with defects, and with a binding energy of  $\approx 2$  eV.<sup>17</sup> Furthermore, evidence from mixed H and D implantations of concentration even greater than in the present tritium implantation indicates that only single atoms are involved in the site.<sup>18</sup> Therefore, the initial state is expected to be atomic tritium rather strongly bound in the silicon lattice in what appears to be a well-defined site.

### 2. Final state

When a free tritium atom decays there is a certain probability that a  $^3\text{He}$  ion will be left in the 1s state, the 2s state, etc., or that the atomic electron will be ejected (shaken off). In the present experiment, however, the final state which is important occurs a "long time" after the decay because the charge collection time in the system is long ( $\sim 6$   $\mu\text{s}$ ). Consequently, the characteristic times for a number of atomic processes need to be considered to determine the final state.

The discussion is somewhat complicated by the lack of knowledge of the binding energies of the electrons to the helium nucleus in a silicon lattice. In the case of muonium,<sup>19-21</sup> the probability density of the electron at the muon is reduced by a factor of 0.45 due to screening from the surrounding electrons of the silicon lattice. This reduction might be accounted for by an effective uniform dielectric constant of 1.3, resulting in an electron

binding energy of about 8 eV. In a somewhat more realistic calculation<sup>20</sup> which takes cognizance of the large macroscopic dielectric constant in silicon, the binding energy is about 1.6 eV. This dielectric effect presumably also operates for  $^3\text{He}^+$  ions, but is probably much less effective for neutral helium, because the two 1s electrons exclude other electrons from around the helium nucleus, and screening only occurs as a result of exchange, as in heavy atoms. This could mean that the binding energy of the 1s electron to the helium nucleus is lower than in the free ion ( $\sim 32$  eV for a uniform dielectric model compared to 54 eV in the free state) and that the binding energy for the second 1s electron is correspondingly larger. (The total electronic binding energy of free  $^3\text{He}$  is 79 eV.)

Now if, in the decay of tritium, the  $^3\text{He}$  ion is left in the 1s state, the high binding energy for the second electron would be expected to lead to rapid neutralization. Bethe and Salpeter<sup>10</sup> have estimated the recombination cross section for hydrogen for eV electrons to be  $\sim 10^{-21}$  cm<sup>2</sup>, varying as the inverse velocity squared, which would lead to recombination lifetimes  $< 10$  ns if applied to the present case. In this estimate, the valence electron density for an interstitial region in silicon<sup>22</sup> has been used.

In the neutralization process, the second electron might go ultimately into the 2s rather than 1s orbital forming what in the free atom is a very long-lived 2S metastable state. What happens in the silicon lattice is not so clear. If the dielectric constant is able to exert its influence as might be anticipated from the muonium results then it is possible that the 2S state is now autoionizing because its binding energy is less than that of  $^3\text{He}^+(1s)$  plus a free electron. The  $^3\text{He}^+(1s)$  ion will then attempt to capture another electron. If the screening due to the silicon electrons is less effective so that the 2s states are bound, it is still likely that the 2S state will decay to the 1S<sub>0</sub> state in a very short time in contrast to the free atom case. This occurs through Auger-type processes in which an electron fills the 1s orbital (from the valence band or from the 2s orbital of  $^3\text{He}$ ) while another electron is ejected. An estimate of this process, using the valence electron density for silicon,<sup>22</sup> leads to lifetimes for these processes of the order of  $10^{-14}$  s (see Appendix B).

If, in the decay, the  $^3\text{He}^+$  ion were left in the 2s state, recombination might be slow or might not occur if the 2S state of the atom were autoionizing. However, the normally metastable 2s state of the ion would decay radiatively quite rapidly because of Stark mixing<sup>10</sup> with the  $2p_{1/2}$  state. The local effective electric field in the detector is about

9000 V/cm which leads to a lifetime estimate of about 1 ns.

The conclusion of all this is that the final state appropriate for this experiment is a neutral  ${}^3\text{He}$  atom in its lowest-energy state in the silicon lattice. The energy released in achieving this situation from that which obtains immediately after the  $\beta$  decay is much larger than the band gap in silicon ( $\sim 1.1$  eV) and will contribute in the usual way to the production of electron-hole pairs and hence to the measured energy.

The uniqueness of the final state reduces the uncertainty in the neutrino mass limit as well and means that in principle a lower limit should be achievable.

### 3. Comparison of ${}^3\text{H}$ - ${}^3\text{He}$ atomic-mass differences

Considering the preceding discussion, the relationship between the extrapolated end-point energy  $Q$  and the  ${}^3\text{H}$ - ${}^3\text{He}$  atomic-mass difference is given by

$$Q = (M_{{}^3\text{H}} - M_{{}^3\text{He}})c^2 - E_{{}^3\text{He}} + E_{{}^3\text{H}}.$$

The additional corrections  $E$  are the energy differences between the silicon lattice with an atom of  ${}^3\text{H}$  or  ${}^3\text{He}$  in it and the silicon lattice plus the free atom. These energies for atomic hydrogen or helium are expected to be a few eV or so<sup>17,23,24</sup>; they will be neglected because their exact values are not at present known. There might also be other small corrections to  $Q$  for incomplete capture of some of the  ${}^3\text{He}$  recoil energy ( $\lesssim 3$  eV) or loss of energy associated with the emission of any photons (from excited helium, for example) whose energy is comparable to the silicon band gap and which therefore may be inefficient in producing particle-hole pairs.

Table V lists the most recent and most accurate end-point energies and  ${}^3\text{H}$ - ${}^3\text{He}$  atomic-mass differences (when available) as well as the most precise mass difference obtained by atomic-mass spectrometry of molecular doublets.<sup>25</sup> The error on the present result contains calibration and statistical uncertainties; as mentioned above it is possible that the end-point energy is systematically low through loss of energy or through a residual pulse-height defect, but it is difficult to see how these sources would exceed 15 eV.

It is presumably fortuitous that the end-point energies in the  $\beta$ -decay experiments all cluster together whereas there is a large spread in values of the  ${}^3\text{H}$ - ${}^3\text{He}$  mass difference. This suggests that there are unaccounted systematic errors in some of the experiments or that their initial- and final-state interpretations are incomplete.

### C. Universal neutrino degeneracy

A universal, degenerate sea of neutrinos or antineutrinos<sup>6</sup> would affect the  $\beta$  spectrum near the end point. In the case of an antineutrino sea,  $\beta^-$  decay would be prevented from occurring with antineutrino energies of less than the Fermi energy of the sea; on the other hand, neutrinos could be captured from a neutrino sea leading to the emission of  $\beta^-$  particles exceeding the extrapolated end-point energy. An analysis similar to that for  $m_{\bar{\nu}}$  gives the 2-standard-deviation limit for both Fermi energies of about 130 eV. (See Appendix A for a simplified discussion of the sensitivity of the measurement to the Fermi energy.) Bergkvist's limits<sup>1</sup> are about 60 eV for both.

At the present, big-bang theories of the origin of the universe suggest that the primordial neutrinos or antineutrinos will not be degenerate, but have a characteristic temperature of a few degrees.<sup>26</sup>

### D. Resolution-function sensitivity

In this type of experiment, an accurate knowledge of the resolution function is very important. There are two aspects to this problem, statistical and systematic. In the present experiment the statistical uncertainty in the resolution is completely negligible and can always be made so by sufficiently intense x-ray sources. A systematic error could occur if the resolution function for an internal  $\beta$  source were not the same as the photopeak resolution for x rays (after allowing for the finite linewidth of the x ray). The importance of this is indicated by the fact that a  $\beta$ -ray resolution 2% better than the x-ray resolution could simulate a 40-eV neutrino mass. A resolution difference might arise in two ways. First, if the  $\beta$  rays and x rays (of the same energy) produced different numbers of electron-hole pairs, then the statistical component of the resolution function would be different, but so would be the pulse height. However, the extrapolated end-point energy probably has an absolute accuracy better than 40 eV and hence the effect on the ratio  $R(m_{\bar{\nu}})$  due to a difference in numbers of electron-hole pairs is  $< 0.05\%$ , i.e., completely negligible. Second, if there is localized radiation damage in the region of the  $\beta$  source it is possible to have incomplete charge collection which may result in broadening and peak distortion as in Fig. 4 and which may be more serious for the  $\beta$  rays than for the x rays. It is evident, moreover, that the x rays can test for radiation damage and that the comparison of the resolution function before implantation with that before and after annealing indicates that more than 95% of the worsening of resolution has been

removed by annealing. To estimate the effect of residual radiation damage on the resolution function, a worst case assumption that the 65 eV end-point energy difference between preannealing and postannealing is due to 50% of the  $\beta$  rays having a pulse-height defect of 130 eV was made. Then assuming that the pulse-height defect is proportional to the residual radiation damage, the worsening of the resolution caused by the defect changes  $R(m_{\bar{\nu}})$  by  $<0.01\%$ , again completely negligible.

The worst case correction for the preannealing runs is a correction downward in  $R(m_{\bar{\nu}})$  of 3%. The experimental agreement between the preannealing and postannealing ratios suggests that the worst case example overestimates the difference between  $\beta$ - and x-ray resolution functions. In any event, the results are essentially unchanged by ignoring the preannealing measurements.

#### E. Radiative corrections

The effect on the  $\beta$  spectrum of an allowed transition due to radiative corrections has been calculated by Sirlin.<sup>27</sup> In this experiment the correction would reduce the number of counts in the sensitive region by a factor of about  $7 \times 10^{-4}$  which is small compared to the present error.

#### VII. CONCLUDING REMARKS

Can the present limit on  $m_{\bar{\nu}}$  from  $\beta$  decay be improved? It has been argued in this paper that an inherent limitation on the accuracy imposed by atomic effects is at a much lower level than in the magnetic-spectrometer measurements, and that the main uncertainty therefore is statistical. The statistical accuracy is strongly influenced by the resolution, the radiation dose that the detector can tolerate, and the length of time which is used for recording the spectrum. In fact, if the present experiment were carried out for one tritium half-life, all other things remaining the same, the limit on  $m_{\bar{\nu}}$  could be reduced to about 20 eV (90% confidence). (One might implant a dozen detectors and count for about a year, achieving again about 20 eV as a limit.) The resolution can be improved only marginally, so that at the moment work is in progress toward an experiment with higher count rate.

There also remains unsettling disagreement in the various determinations of the  $^3\text{H}$ - $^3\text{He}$  mass difference. A check on the extrapolated end-point energy for the present experiment is to be attempted by a very low dose implantation, avoiding as much as possible effects of radiation damage. Further study of the nature of helium in a silicon lattice would also seem to be interesting.

A preliminary report<sup>29</sup> has appeared giving  $m_{\bar{\nu}} = 34 \pm 4$  eV, and a 99% confidence interval from 14 to 46 eV. Unfortunately, the authors do not comment on the apparent discrepancy of their new result with that of their first publication.<sup>3</sup>

#### ACKNOWLEDGMENTS

The author gratefully acknowledges the interest, informative conversations and help of J. L. Campbell, W. R. Dixon, P. A. Egelstaff, G. Karl, A. B. McDonald, J. R. MacDonald, I. K. MacKenzie, B. G. Nickel, P. Peercy, R. S. Storey, and I. Towner. He also especially thanks J. A. Kuehner and his staff at the McMaster Tandem Accelerator Laboratory for assistance in the implantation of the tritium, and J. Law for his contribution to Appendix B. This work was funded under a grant from the National Research Council of Canada and the Natural Sciences and Engineering Research Council of Canada, Grant No. A-6024.

#### APPENDIX A

In this appendix a simplified analysis of the sensitivity of the present method will be given.

The main problem of this method is the poor resolution of the Si(Li) x-ray detector. As a result of this, the "missing counts" near the end point due to a finite neutrino mass are spread over a region comparable to the resolution. Rather than including the complication of the resolution function in the present qualitative discussion, the  $\beta$  spectrum without resolution folded in will be used but a region  $\Delta E$  near the end point which is much larger than  $m_{\bar{\nu}}$  will be taken as the analysis region. It has been found from the exact computer calculations in which the resolution function has been folded in that the size of  $\Delta E$  giving the most sensitivity (as measured by statistical accuracy relative to the effect of the neutrino mass) is about twice the detector full width at half maximum.

As in Eq. (1) the number of counts in the  $\beta$  spectrum  $N_{\beta}(E, Z)$  is given by

$$N_{\beta}(E, Z) \propto pE[(Q-E)^2 - m_{\bar{\nu}}^2]^{1/2}(Q-E)F(E, Z). \quad (\text{A1})$$

The area in the spectrum in a region  $\Delta E$  below the extrapolated end point  $Q$  is

$$A(m_{\bar{\nu}}) \propto \int_{Q-\Delta E}^Q N_{\beta}(E, Z) dE.$$

Considering the product  $pEF(E, Z)$  to be constant over this region, the area is

$$A(m_{\bar{\nu}}) \propto (\Delta E^2 - m_{\bar{\nu}}^2)^{3/2} \quad (\text{A2})$$

and therefore the ratio corresponding to that shown in Fig. 7 is

$$R(m_{\bar{\nu}}) = \frac{A(m_{\bar{\nu}})}{A(0)} = \left(1 - \frac{m_{\bar{\nu}}^2}{\Delta E^2}\right)^{3/2}. \quad (\text{A3})$$

For example, given  $\Delta E = 600$  eV and  $m_{\bar{\nu}} = 100$  eV,  $R = 0.959$ , in good agreement with the exact computer calculations of Fig. 7.

The above analysis can be extended to examine which combination of detector size and resolution is advantageous for achieving a certain limit on  $m_{\bar{\nu}}$  in a given time under the constraint of a certain fluence (implantation dose per unit area). For small neutrino mass, the area after a certain counting time  $t$  at a counting rate  $C$  is essentially  $\propto tC\Delta E^3$  and hence the relative standard deviation is  $\propto (tC\Delta E^3)^{-1/2}$ , neglecting background. The count rate is proportional to the detector area  $A$  for a given fluence, and  $\Delta E$  (which depends on the resolution) is also a slow function of  $A$ . Consequently, specifying the limit on  $m_{\bar{\nu}}$  by the requirement that a multiple  $f$  of the relative standard deviation should be less than  $R(0) - R(m_{\bar{\nu}})$  leads to the criterion

$$t \propto f^2 \frac{\Delta E}{Am_{\bar{\nu}}^4}. \quad (\text{A4})$$

This expression displays a couple of important points. Firstly, the time to achieve a certain limit  $m_{\bar{\nu}}$  increases inversely as the fourth power of  $m_{\bar{\nu}}$ , emphasizing the difficulty of lowering the limit. Secondly, the time required depends on the ratio  $\Delta E/A$ , but the change in  $\Delta E$  with  $A$  is very small for commercially available detectors. For example, 30-mm<sup>2</sup> detectors have a resolution of about 210–230 eV at 18 keV, whereas in 80-mm<sup>2</sup> detectors the resolution ranges from about 250–300 eV. Therefore, the time to achieve a certain limit decreases with increasing  $A$ .

One can also investigate the sensitivity of the result to several discrete final states. Suppose that there were two final states of energy  $Q$  and  $Q - \Delta Q$  (where  $Q$  is as defined in the text) of relative proportions  $(1 - \alpha)$  and  $\alpha$ . Away from the end region, the results are insignificantly changed provided one defines the extrapolated end-point energy to be the weighted average  $\bar{Q}$  and provided  $\Delta Q$  is small. The  $\beta$  spectrum in this case is (for  $m_{\bar{\nu}} = 0$ )

$$N(E) \propto pE[(\bar{Q} - E)^2 + \alpha(1 - \alpha)\Delta Q^2]. \quad (\text{A5})$$

At the end point, the area in a region  $\Delta E$  below  $Q$  will be changed; the fractional increase in area for two final states relative to one is  $3\alpha(1 - \alpha) \times \Delta Q^2/\Delta E^2$ . If one assumed two final states when in reality there was only one, the difference in area could be duplicated by a neutrino mass  $m_{\bar{\nu}}$

of magnitude  $[2\alpha(1 - \alpha)]^{1/2}\Delta Q$ . Thus, if  $\alpha$  is unknown, the effective limit obtainable for the neutrino mass is  $\sim 0.7 \Delta Q$ .

Finally, consider the possibility of either a universal antineutrino or neutrino degeneracy.<sup>1,6</sup> In the first case, the  $\beta^-$  spectrum terminates abruptly at an energy of  $Q - E_F(\bar{\nu})$ , where  $E_F(\bar{\nu})$  is the antineutrino Fermi energy (although the extrapolated end point is still  $Q$ ). Hence, the area in the sensitive region  $\Delta E$  is proportional to

$$\Delta E^3 \left[1 - \frac{E_F(\bar{\nu})^3}{\Delta E^3}\right].$$

In the case of neutrino degeneracy,  $\beta^-$  particles can be emitted with energies greater than  $Q$  and the  $\beta$  spectrum rises from  $Q$  to  $Q + E_F(\nu)$  with the same shape as from  $Q$  to  $Q - E_F(\bar{\nu})$ . Consequently, the area is proportional to

$$\Delta E^3 \left[1 + \frac{E_F(\nu)^3}{\Delta E^3}\right].$$

In both cases one sees that the analysis is less sensitive to neutrino degeneracy than to neutrino mass.

#### APPENDIX B

An isolated He atom has long-lived 2S metastable states. (For example, the 2<sup>3</sup>S state has a lifetime of 7 s.) Supposing a He atom to be in a 2S state when introduced into the Si lattice, the rate of deexcitation of this state would be of interest. This state could deexcite by a process which might be called an interatomic Auger effect. In the lattice one can imagine a process in which the 2s electron drops into the 1s orbital with the simultaneous ejection of a valence electron of Si (direct process) or an exchange process in which the He 2s electron is ejected and a Si electron is captured into the He 1S state.

Although in a silicon lattice orbitals will form which are an admixture of the valence levels of the Si atoms and the He levels, the calculations of Kaplan *et al.*<sup>28</sup> show that, at least for the 1S state of He, the mixing is not terribly strong. For the estimation of the interatomic Auger processes, it is therefore assumed that the atomic states of Si and He are unaffected by the presence of the latter in the lattice. The rate of these processes is proportional to the matrix elements

$$\int \frac{[\phi^*(\vec{k}_f, \vec{r}_2)e\phi(\vec{k}_i, \vec{r}_2)][\psi_{1s}^*(\vec{r}_1)e\psi_{2s}(\vec{r}_1)]}{|\vec{r}_1 - \vec{r}_2|} d^3r_1 d^3r_2 \quad (\text{direct})$$

and

$$\int \frac{[\psi_{1s}^*(\vec{r}_2)e\phi(\vec{k}_i, \vec{r}_2)][\phi^*(\vec{k}_f, \vec{r}_1)e\psi_{2s}(\vec{r}_1)]}{|\vec{r}_1 - \vec{r}_2|} d^3r_1 d^3r_2$$

(exchange).

The He 1s electron is treated as a spectator. (The first expression is similar to monopole internal conversion.)

In order to simplify the calculations the following approximations are used.

(a) The wave function of the Si valence electron  $\phi(\vec{k}_i, \vec{r})$  is considered to be a plane wave of momentum  $\vec{k}_i = 0$ . The normalization is chosen to fit the valence electron density in Si.<sup>22</sup>

(b) The final-state continuum wave function is also a plane wave  $\phi(\vec{k}_f, \vec{r})$ .

(c) The final-state He 1s wave function is taken to be a hydrogenic wave function with  $Z = 2$ ; i.e., the radial part is

$$\psi_{1s}(r) = \frac{2^{5/2}}{a_0^{3/2}} e^{-2r/a_0},$$

where  $a_0$  is the Bohr radius.

(d) The He 2s wave function of the initial state is based on a hydrogenic 1s wave function with  $Z = 1$ , but made orthogonal to the final state by the addition of an  $e^{-2r/a_0}$  component. Specifically

$$\psi_{2s}(r) = \frac{2}{a_0^{3/2}} \left(1 - \frac{8^3}{2 \cdot 7^2}\right)^{-1/2} \left(e^{-r/a_0} - \frac{64}{27} e^{-2r/a_0}\right).$$

Because the interaction is of monopole type, the spherical part of the plane-wave expansion

$$\exp\left(\frac{i\vec{k} \cdot \vec{r}}{\hbar}\right) = \frac{\sin(kr/\hbar)}{(kr/\hbar)}$$

is used. With the above approximations, the integration of the matrix elements can be carried out analytically. The transition rates can be expressed in terms of the dimensionless parameter  $qa_0/\hbar \equiv \gamma$ , where  $\vec{q}$  is the momentum transfer ( $\vec{q} = \vec{k}_f - \vec{k}_i \approx \vec{k}_f$ , here). With this notation, the direct rate is

$$T = \frac{4.0 \times 10^{21}}{\gamma^2} \left[1 - \left(\frac{16}{9}\right)^2 \left(\frac{9 + \gamma^2}{16 + \gamma^2}\right)^2\right]^2$$

$$\times \frac{4}{(9 + \gamma^2)^4} \frac{n}{[R(\text{\AA})]^3} \text{ s}^{-1}.$$

Here  $n$  is the silicon valence electron density in electrons per unit cell and  $R$  ( $\text{\AA}$ ) is the unit cell dimensions in angstroms. The exchange transition rate is a more complicated expression, but leads to a similar order of magnitude for  $\gamma$  values of interest, i.e.,  $\gamma \approx 1$ . With  $\gamma = 1.33$  (corresponding to 20 eV between metastable and ground state),  $n = 4$ ,<sup>22</sup> and  $R = 5.4 \text{ \AA}$ , the direct lifetime is about  $1.3 \times 10^{-14}$  s and the exchange lifetime is about  $4.9 \times 10^{-15}$  s.

<sup>1</sup>K-E. Bergkvist, Nucl. Phys. **B39**, 317 (1972); **B39**, 371 (1972); Phys. Scr. **4**, 23 (1971).

<sup>2</sup>W. F. Piel, Nucl. Phys. **A203**, 369 (1973).

<sup>3</sup>E. F. Tret'yakov, N. F. Myasoedov, A. M. Apalikov, V. F. Konyaev, V. A. Lyubimov, and E. G. Novikov, Bull. Acad. Sci. USSR, Phys. Ser. **40**, 1 (1976).

<sup>4</sup>J. J. Simpson, in *Neutrino '79*, proceedings of the International Conference on Neutrinos, Weak Interactions, and Cosmology, Bergen, Norway, 1979, edited by A. Haatuft and C. Jarlskog (Univ. of Bergen, Bergen, 1979), Vol. 2, p. 208.

<sup>5</sup>V. E. Lewis, Nucl. Phys. **A151**, 120 (1970).

<sup>6</sup>S. Weinberg, Phys. Rev. **128**, 1457 (1962).

<sup>7</sup>F. S. Goulding and D. A. Landis, IEEE Trans. Nucl. Sci. **NS-25**, 896 (1978).

<sup>8</sup>R. Gunnink, R. A. Meyer, J. B. Niday, and R. P. Anderson, Nucl. Instrum. Methods **65**, 26 (1968).

<sup>9</sup>H. F. Schopper, *Weak Interactions and Nuclear Beta Decay* (North-Holland, Amsterdam, 1966).

<sup>10</sup>H. A. Bethe and E. E. Salpeter, in *Encyclopedia of Physics*, edited by S. Flugge (Springer Berlin 1957) Vol. XXXV, p. 88.

<sup>11</sup>H. J. Hovel, *Semiconductors and Semimetals* (Academic, New York, 1975), Vol. II.

<sup>12</sup>Purchased from Princeton Gamma Tech. One disadvantage of the pulsed optical-feedback preamplifier is that the x-ray event which causes the reset is lost and this makes the detector's efficiency energy dependent,

especially for large energies near the reset energy.

This effect has been investigated experimentally and statistically [E. M. Carter, Dept. of Mathematics and J. Law, Dept. of Physics, University of Guelph and I. Towner, Chalk River Nuclear Laboratories (unpublished)] and a correction has been applied (see text).

<sup>13</sup>J. A. Bearden, Rev. Mod. Phys. **39**, 78 (1967).

<sup>14</sup>J. H. Scofield, Phys. Rev. A **9**, 1041 (1974).

<sup>15</sup>P. Marmier and C. Sheldon, *Physics of Nuclei and Particles* (Academic, New York, 1969), Vol. 1, p. 360.

<sup>16</sup>H. Behrens and J. Jänecke, *Landolt-Börnstein New Series* (Springer, Berlin, 1969), Group I, Vol. 4.

<sup>17</sup>S. T. Picraux, F. L. Vook, and H. J. Stein, in *Proceedings of the International Conference on Defects and Radiation Effects in Semiconductors, Nice, France, 1978*, edited by J. H. Albany (Institute of Physics, Bristol, England, 1979), p. 31.

<sup>18</sup>S. T. Picraux and F. L. Vook, Phys. Rev. B **18**, 2066 (1978).

<sup>19</sup>J. H. Brewer, K. M. Crowe, F. N. Gygas, R. F. Johnson, and B. D. Patterson, Phys. Rev. Lett. **31**, 143 (1973).

<sup>20</sup>J. Shy-Yih Wang and C. Kittel, Phys. Rev. **137**, 713 (1973).

<sup>21</sup>M. Altarelli and W. H. Hsu, Phys. Rev. Lett. **43**, 1346 (1979).

<sup>22</sup>V. H. Smith, Jr., Phys. Scr. **15**, 147 (1977).

<sup>23</sup>B. I. Boltaks, *Diffusion in Semiconductors* (Academic,

- New York, 1963).
- <sup>24</sup>E. V. Kornelson, National Research Council Canada (private communication).
- <sup>25</sup>L. G. Smith and A. H. Wapstra, *Phys. Rev. C* 11, 1392 (1975).
- <sup>26</sup>G. Steigman, in *Unification of Elementary Forces and Gauge Theories*, proceedings of the Ben Lee Memorial Conference, Fermilab, 1977, edited by D. B. Cline and F. E. Mills (Harwood Academic, London, 1979), p. 453.
- <sup>27</sup>A. Sirlin, *Phys. Rev.* 164, 1767 (1967).
- <sup>28</sup>D. R. Kaplan, C. Weigel, and J. W. Corbett, *Phys. Status Solidi B* 94, 359 (1979).
- <sup>29</sup>V. A. Lyubimov, E. G. Novikov, V. Z. Nozik, E. F. Tret'yakov, and V. S. Kosik, *Phys. Lett.* B94, 266 (1980).